JOURNAL OF SPACECRAFT AND ROCKETS
Vol. 34, No. 2, March–April 1997

Periodic Optimal Cruise for a Hypersonic Vehicle with Constraints

C.-H. Chuang* and Hitoshi Morimoto†
Georgia Institute of Technology, Atlanta, Georgia 30332-0150

A new approach is presented to solve periodic optimal control problems. As an application of the approach, fuel-optimal periodic control problems for a hypersonic vehicle are solved. The model of the vehicle was constructed by using numerical data and figures from available space plane literature. In particular, heating-rate and load-factor constraints are considered to make this model more realistic than other previous models. These constraints increase the difficulty in obtaining a numerical solution and also increase the sensitivity to the initial guess for convergence. By assuming the shape of an altitude profile as a sinusoidal function of range and by using a bang-bang thrust control, a suboptimal solution is obtained for the vehicle without any constraints. This suboptimal solution serves as a very good initial guess for the optimal solution generated by the minimizing-boundary-conditionmethod. The optimal solution shows a fuel saving of 8.12% over the steady-state cruise, with a maximum heating rate of 1202.4 W/cm^2, and with a maximum load factor of 8.27. Constraints for a heating rate and a load factor are then added to the problem. With a maximum heating rate of 400 W/cm^2, the fuel saving reduces to 2.45%. With a load factor of 7, the fuel saving does not change much from the nonconstrained solution. An optimal periodic-cruise solution with maximum heating rate of 1158.0 W/cm^2 and simultaneously with maximum load factor of 7 is also determined with a fuel saving of 8.09%.

Nomenclature

A_e = inlet area, m^2
A_w = wing area, m^2
a = speed of sound at sea level or at the standard temperature, m/s
b_j = lapse rate between jth and $(j+1)$th junction points, where j is 0, 2, 4, and 6
C = load factor constraint function
C_D = drag coefficient
C_{D_0} = zero-lift drag coefficient
C_L = lift coefficient
C_{L_0} = zero angle-of-attack lift coefficient
C_{L_α} = lift-curve slope
$C_{T\max}$ = maximum thrust coefficient
D = drag, N
$\boldsymbol{f}$ = system dynamics vector
g = gravity acceleration at sea level, m/s^2
h = altitude, km
h_a = amplitude corresponding to frequency ω of a specified sinusoidal altitude curve
h_b = amplitude corresponding to frequency 2ω of a specified sinusoidal altitude curve
h_c = offset of a specified sinusoidal altitude curve
I_{sp} = specific impulse, s
J = cost function
K = induced drag parameter
L = lift, N
M = Mach number (defined as a normalized velocity by a constant speed of sound at sea level)
m = mass of the vehicle, kg
n = load factor
$n_{\max}$ = specified maximum load factor
$\dot{Q}$ = heating rate, W/cm^2
$\dot{Q}_{\max}$ = specified maximum heating rate, W/cm^2
q = dynamic pressure, N/m^2
R = specific gas constant for air, J/kgK
R_0 = radius of the Earth, km
r = range, km
r_d = coordinate of range where a specified throttle falls from 1 to 0
r_u = coordinate of range where a specified throttle rises from 0 to 1
r_1 = coordinate of range of an entry point to a boundary
S = heating-rate constraint function
s = throttle
T = thrust, N
T_i = temperature at ith junction point, where i is 0, 1, 2, 3, 4, 5, and 6, K
$\boldsymbol{u}$ = control vector
V = velocity, m/s
$\boldsymbol{x}$ = state vector
α = angle of attack, deg
γ = flight-path angle, deg
$\boldsymbol{\lambda}$ = Lagrange multiplier vector
μ = Lagrange multiplier function associated with a load-factor constraint
ν = Lagrange multiplier constant associated with periodic boundary condition on the state
ξ = Lagrange multiplier function associated with a heating-rate constraint
π = Lagrange multiplier constant associated with heating rate constraint at an entry point
ρ = density of air, kg/m^3
ω = frequency with respect to range of a specified sinusoidal altitude curve

Received Nov. 30, 1995; revision received Oct. 15, 1996; accepted for publication Nov. 12, 1996.

*Part-time Associate Professor, School of Aerospace Engineering. Senior Member AIAA.
†Graduate Student, School of Aerospace Engineering.

Introduction

EVER since improved fuel efficiency for some oscillatory cruise paths over that for steady-state cruise paths was first recognized,[1] research on periodic optimal processes has been an active subject, especially for fuel saving for aircraft and hypersonic vehicles.[2–13] Fuel-optimal periodic trajectories without constraints were numerically determined for aircraft and hypersonic vehicles.[7–13] An optimal periodic control problem for a hypersonic vehicle with a maximum load-factor constraint was recently solved.[13] Those studies, however, did not consider the aerodynamic heating that vehicles would experience along the optimal trajectories. Thus, to protect the crew and materials of the vehicle from the heat, it is necessary to impose a restriction on the heating rate. This restriction means that the periodic optimal control problem must be

solved with a state inequality constraint associated with the heating-rate constraint, and the problem becomes more difficult to solve.

This paper has two parts. One is about a new approach to attack periodic optimal control problems with constraints. The other is about an application of the approach to fuel-optimal periodic control problems for a realistic hypersonic vehicle model.

In the following sections, the vehicle's dynamics are stated and the atmospheric density model, the aerodynamic force models, and the engine thrust model are described. A more realistic aircraft model and a more precise atmospheric model than previously used models are adopted here. An approximation to the optimal control solution was obtained by parameterizing the control time histories and using nonlinear programming techniques to obtain the optimum values of the parameters. This solution, which we call a suboptimal solution, in turn was used as an initial guess in solving the optimal control problem. The unconstrained optimal periodic solution shows that the vehicle has a peak aerodynamic heating rate of over 1200 W/cm^2 and a peak load factor of over 8 g along the optimal trajectory. We next present an optimal periodic control solution constrained by a maximum load factor of 7.0 g and another solution constrained by a maximum heating rate of 400 W/cm^2. The load factor constraint constitutes a state-control inequality constraint, and the maximum heating rate constitutes a state inequality constraint. Finally, an optimal periodic control solution is presented with both a maximum load factor and a maximum heating-rate constraint.

Vehicle's Dynamic Model

The equations of motion for flight in a vertical plane over the nonrotating spherical Earth with range as the independent variable are[10]

$$\frac{\mathrm{d}h}{\mathrm{d}r} = (\tan\gamma)\left(1 + \frac{h}{R_0}\right) \tag{1}$$

$$\frac{\mathrm{d}M}{\mathrm{d}r} = \frac{(T\cos\alpha - D - mg\sin\gamma)}{Ma^2 m\cos\gamma}\left(1 + \frac{h}{R_0}\right) \tag{2}$$

$$\frac{\mathrm{d}\gamma}{\mathrm{d}r} = \left(\frac{L + T\sin\alpha - mg\cos\gamma}{M^2a^2m\cos\gamma} + \frac{1}{R_0 + h}\right)\left(1 + \frac{h}{R_0}\right) \tag{3}$$

$$\frac{\mathrm{d}m}{\mathrm{d}r} = -\frac{T}{gI_{\mathrm{sp}}Ma\cos\gamma}\left(1 + \frac{h}{R_0}\right) \tag{4}$$

Although the derivative of m with respect to r is given in Eq. (4), the mass in Eqs. (1–3) is assumed to be constant. Thus, the components of the state are h, M, and γ only.

Atmospheric Density Model

Instead of using a simple exponential density model, we adopt an atmospheric density model in which temperature changes are taken into account. The density model is based on the temperature distribution with respect to altitude.[14]

Take fixed points $(h_0, T_0) = (0, 288.16)$, $(h_1, T_1) = (11, 216.66)$, $(h_2, T_2) = (25, 216.66)$, $(h_3, T_3) = (47, 282.66)$, $(h_4, T_4) = (53, 282.66)$, $(h_5, T_5) = (79, 165.66)$, $(h_6, T_6) = (90, 165.66)$, and $(h_7, T_7) = (105, 225.66)$ in h–T plane. Assume piecewise linear interpolation of temperature as a function of altitude. In the isothermal region the density becomes an exponential function of the form

$$\rho = \rho_i \exp[-(g/RT_i)(h - h_i)] \tag{5}$$

In the gradient layer region the density is given by

$$\rho = \rho_j\left(\frac{T_j + b_j(h - h_j)}{T_j}\right)^{-[(g/b_jR)+1]} \tag{6}$$

We assume that the gradient layer region from $h = 90$ to 105 km is extrapolated up to $h = 120$ km. To avoid numerical error of calculating derivatives of the density models with respect to altitude at the junction points of the models, each junction point in the density curve is smoothed by third-order polynomials.

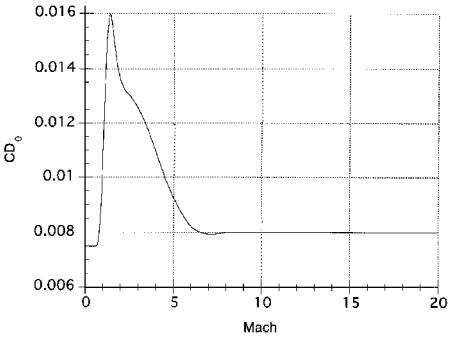

Fig. 1 $C_{D_0}(M)$.

Aerodynamic Force Models

The drag and lift models are assumed to have the following forms:

$$D = q \cdot C_D \cdot A_w \tag{7}$$

$$L = q \cdot C_L \cdot A_w \tag{8}$$

$$C_D = C_{D_0}(M) + K(M) \cdot C_L^2 \tag{9}$$

$$C_L = C_{L_0}(M) + C_{L_\alpha}(M) \cdot \alpha \tag{10}$$

Functions $C_{D_0}(M)$, $K(M)$, $C_{L_0}(M)$, and $C_{L_\alpha}(M)$ are determined by modifying experimental and simulation data.[15–17] Because Ref. 15 deals with experimental aerodynamic characteristics of HL-20, whose nose cone is more blunt than that of a typical space plane, we have modified C_{D_0} and C_{L_0} in Ref. 15 as follows:

$$C_{D_0} \to \tfrac{1}{10}C_{D_0} \qquad C_{L_0} \to C_{L_0} + 0.04$$

$C_{D_0}(M)$ is shown in Fig. 1. $K(M)$, $C_{L_0}(M)$, and $C_{L_\alpha}(M)$ are explicitly written in the following forms:

$$K(M) = 1.85 \cdot [1 - \exp(-0.2356M)]$$

$$C_{L_0}(M) = (1/20\pi)\tan^{-1}[10(M - 1)] - 0.035$$

$$C_{L_\alpha}(M) = 0.057 \cdot \exp(-0.654M) + 0.014$$

Engine Model

A combination of turboramjet engines and scramjet engines is assumed for the propulsion system of the vehicle. From $M = 0$ to 4 the turboramjet is turned on, and for $M > 4$ the scramjet engine propels the vehicle. The maximum thrust coefficient $C_{T\max}$ and specific impulse I_{sp} are modeled as functions of altitude h, Mach number M, and angle of attack α. In determining I_{sp} and $C_{T\max}$, data from Refs. 18–20 are averaged. The coefficients in Eqs. (11) and (13) are obtained by curve fitting to those data:

$$C_{T_{\max}}(M, \alpha) =$$

$$\begin{cases} 0.4736M^{1.5} + 1.6947M^{-2} & (M < 4) \\ \dfrac{15(\alpha + 5)^{0.25}}{M^{1.15}} \exp\left\{-\dfrac{M^{0.08}}{200}\left[(\alpha + 5) - \dfrac{35}{M^{0.6}}\right]^2\right\} & (M \geq 4) \end{cases} \tag{11}$$

$$T = sqC_{T_{\max}}A_e \qquad (0 \leq s \leq 1) \tag{12}$$

$$I_{\mathrm{sp}}(h, M) = \begin{cases} 4500 - 10(h - 20) & (M < 4) \\ -245M + 5480 - 10(h - 20) & (M \geq 4) \end{cases} \tag{13}$$

Optimal Steady-State Cruise Solution

By setting Eqs. (1–3) equal to zero, the steady-state solutions are calculated. The solutions determine the angle of attack and throttle as functions of h and M,

$$\alpha = \alpha(h, M) \qquad \text{and} \qquad s = s(h, M)$$

The range averaged fuel consumption rate is given by

$$J = \frac{1}{r_f}\int_0^{r_f} \frac{T}{gI_{sp}Ma\cos\gamma}\left(1+\frac{h}{R_0}\right)\mathrm{d}r \tag{14}$$

On steady-state cruise paths the range averaged fuel consumption rate J becomes an instantaneous fuel-consumption rate

$$J = \frac{1}{r_f}\int_0^{r_f} \frac{\tilde{T}(h,M)}{gI_{sp}(h,M)}\frac{1}{Ma}\left(1+\frac{h}{R_0}\right)\mathrm{d}r$$

$$= \frac{\tilde{T}(h,M)}{gI_{sp}(h,M)Ma}\left(1+\frac{h}{R_0}\right) \tag{15}$$

where

$$\tilde{T}(h,M) = T[h,M,\alpha(h,M),s(h,M)]$$

Thus, the optimal steady-state cruise path is determined by finding an (h, M) that minimizes Eq. (15). Note that the minimization must be done within an admissible (h, M) that satisfies an inequality constraint on s

$$0 \le s(h,M) \le 1 \tag{16}$$

For the numerical constants $R_0 = 6378$ km, $m = 89{,}930$ kg, $g = 9.80665$ m/s^2, $a = 340.294$ m/s, $R = 287$ J/kgK, $A_w = 250$ m^2, and $A_e = 9.02$ m^2, the optimal steady-state cruise turned out to be as follows: $h = 42376$ m, $M = 14.37$, $\alpha = 5.34$ deg, $s = 0.3668$, and minimum fuel rate $= 0.001555$ kg/m.

Suboptimal Periodic-Cruise Solution

In this section we obtain an approximation to the optimal periodic control solution by parameterizing the control time histories and using nonlinear programming to determine the optimum values of the parameters. This solution will be used as an initial guess for the optimal control problem in the next section. Because the optimal control problems that will be solved in the next section are very sensitive to initial guesses, it is very desirable to have a good initial guess from the beginning.

Previous results show that the optimal periodic trajectory usually has a sinusoidal-like shape.[7,8,10] If a trajectory is given as a sinusoidal curve and a bang-bang type throttle control is assumed, then the range averaged fuel consumption can be calculated in terms of the parameters that specify the trajectory and throttle control. The problem herein is to find a set of parameters that minimizes the range averaged fuel consumption rate Eq. (14) with the boundary condition of periodicity being met.

The altitude h is assumed to take the following expression as a function of range:

$$h = h_a\cos\omega r + h_b\cos 2\omega r + h_c \tag{17}$$

and ω is determined by the length of a period r_f as $\omega = 2\pi/r_f$. From Eqs. (1) and (17),

$$\gamma = -\tan^{-1}\left[\frac{\omega(h_a\sin\omega r + 2h_b\sin 2\omega r)}{1+h/R_0}\right] \tag{18}$$

A bang-bang type throttle control is specified by choosing two switching points whose coordinates are r_u and r_d. From $r = 0$ to r_u the throttle is equal to 0, from $r = r_u$ to r_d it is equal to 1, and from $r = r_d$ to r_f, or the end of the period, it is equal to 0 again. The parameters to be optimized are h_a, h_b, h_c, r_f, r_u, r_d, and M_0, which is the initial Mach number. From Eqs. (1), (3), (17), and (18) we obtain an equation for the angle of attack. An analytical form for the angle of attack is not available from this algebraic equation, and hence, the angle of attack is determined by solving the equation numerically. Starting from an M_0 and substituting the angle of attack and the specified throttle's time history into Eq. (2), a final Mach number M_f is calculated by integrating Eq. (2) numerically from $r = 0$ to r_f. The periodicity boundary condition requires that M_f is equal to M_0. Note that the other two periodicity conditions, $h_0 = h_f$ and $\gamma_0 = \gamma_f$, are automatically satisfied by Eqs. (17) and (18).

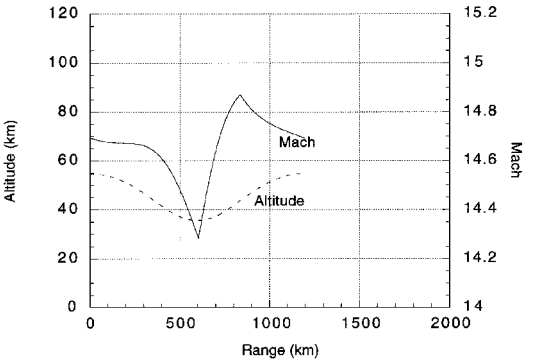

Fig. 2 Altitude and Mach number M, suboptimal.

NCONF, a nonlinear programming subroutine of IMSL, was used to find a set of parameters $h_a, h_b, h_c, r_f, r_u, r_d$, and M_0 that minimizes Eq. (14) subject to $M_0 = M_f$. The profiles of the altitude and Mach number M are shown in Fig. 2.

The range averaged fuel consumption rate for the suboptimal solution is 0.001501 kg/m, which is about 3.5% less than the steady-state solution. The optimized parameters are listed as follows: $h_a = 9551$ m, $h_b = -810$ m, $h_c = 45{,}942$ m, $r_f = 1{,}194{,}041$ m, $r_u = 603{,}606$ m, $r_d = 835{,}062$ m, and $M_0 = 14.694$.

Optimal Periodic-Cruise Solution Without Constraint

In this section we obtain the unconstrained optimal periodic-cruise solution using a suboptimal solution that was obtained in the preceding section. The suboptimal solution is used as an initial guess for the optimal control problem.

In Eq. (14) the range averaged fuel consumption rate was given by

$$J = \frac{1}{r_f}\int_0^{r_f} \frac{T}{gI_{sp}Ma\cos\gamma}\left(1+\frac{h}{R_0}\right)\mathrm{d}r \tag{14}$$

The Hamiltonian for the cost function J and the system subject to Eqs. (1–3) is written as

$$H = \frac{T}{gI_{sp}Ma\cos\gamma}\left(1+\frac{h}{R_0}\right) + \boldsymbol{\lambda}^T\cdot\boldsymbol{f}$$

where $\boldsymbol{\lambda}$ consists of $\boldsymbol{\lambda}_h$, $\boldsymbol{\lambda}_M$, and $\boldsymbol{\lambda}_\gamma$ and the components of $\boldsymbol{f}$ are Eqs. (1–3).

The first-order necessary conditions for the optimal solution are obtained as follows[7]:

$$\frac{\mathrm{d}\boldsymbol{x}^T}{\mathrm{d}r} = H_\lambda \tag{19}$$

$$\frac{\mathrm{d}\boldsymbol{\lambda}^T}{\mathrm{d}r} = -H_x \tag{20}$$

$$\boldsymbol{u} = \arg\min_u H \tag{21}$$

$$\boldsymbol{x}(r_f) = \boldsymbol{x}(r_0), \qquad \boldsymbol{\lambda}(r_f) = \boldsymbol{\lambda}(r_0) \tag{22}$$

$$H(r_f) = J^o \tag{23}$$

J_o in Eq. (23) is calculated by Eq. (14) along the optimal solution.

When this type of problem is solved as a two-point boundary-value problem by using a shooting method, the convergence of the solution is very sensitive to the choice of initial guesses of both states and costates. Thus, it is very important to select a proper initial guess. We use the suboptimal solution as an initial guess for the states. However, an initial guess for the costates is not provided by the suboptimal solution. Initial values of $\boldsymbol{\lambda}$ can be estimated as follows. At the initial point of r the Hamiltonian H is written as

$$H(r_0) = L(r_0) + \boldsymbol{\lambda}^T(r_0)\boldsymbol{f}(r_0) \tag{24}$$

where L is the Lagrangian that is equal to the integrand of Eq. (14). From Eq. (24) the following holds:

$$\frac{\partial H}{\partial \boldsymbol{f}}_{r=r_0} = \boldsymbol{\lambda}^T(r_0) \tag{25}$$

The cost function J^o is equal to $H(r_f)$ when a solution is optimal, and H is constant for an autonomous system. Hence,

$$\frac{\partial J^o}{\partial \boldsymbol{f}}_{r=r_0} = \boldsymbol{\lambda}^T(r_0) \tag{26}$$

Now assume that the suboptimal solution is approximately close to the optimal solution.

The procedure for determining the optimal solution is described as follows (steps 2 and 3 are based on Ref. 10).

1) Obtain an initial guess for the states and the costates by the suboptimal solution and Eq. (26).

2) Starting with the initial guess, final states and costates are calculated by integrating Eqs. (1–3) and (20) numerically. Without loss of generality we can choose $\gamma_0 = 0$. The integration is stopped when γ becomes zero again. Define a cost function $P = (M_f - M_0)^2$. By observing the initial guess and the resulting final states and costates, a nonlinear programming subroutine, NCONF, for example, generates a new initial guess to decrease P subject to the boundary conditions excepting $M_f - M_0 = 0$. From this new initial guess, final states and costates are calculated again. The nonlinear programming subroutine repeats this process until P is close to zero while the other boundary conditions are satisfied.

3) If a solution is obtained from step 2, take the point as a new initial guess and add another boundary condition Eq. (23). Start the minimization of P with the new initial guess.

4) If a convergence is obtained in step 3, the optimal solution is determined. If step 3 does not converge, apply one of the initial guesses that were generated by the optimization program in step 3. Use this initial guess and repeat step 2.

In Fig. 3, initial altitude and initial Mach number M of each periodic solution are plotted. Point A is the starting point (step 1). According to the procedure just stated, point B is reached (step 2), which belongs to a family of periodic extremal paths satisfying Eqs. (19–22). The curve drawn in Fig. 3 shows a family of the periodic extremal paths. Use point B as an initial guess and include the transversality condition Eq. (23) to reach the optimal solution (step 3). If point B is close to the optimal solution (point G), then the optimal solution will converge. However, if point B is not close enough to G, the optimization algorithm may stray in the wrong direction and the searching process could terminate. If the search terminates, use one of the points that were generated by the optimization program before it stopped as a next initial guess (points C and E are as such points in Fig. 3). Restart the optimization algorithm without imposing the transversality condition (step 4). The algorithm should find another solution that is in the solution family. Points D and F show those solutions. By repeating this process the optimal solution is obtained. Note here, however, that in general there is no guarantee that a continuous flow of solutions always exists. Solutions obtained by the continuation method may not be optimal.

The profiles of the altitude and Mach number are plotted in Fig. 4. The fuel saving of the solution over the optimal steady-state solution was 8.12%. The numerical solution showed that the boundary conditions are satisfied up to at least 11 significant digits.

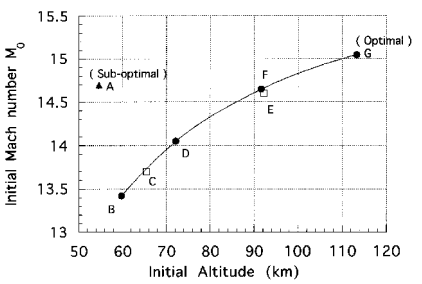

Fig. 3 Path to the optimal solution without constraint.

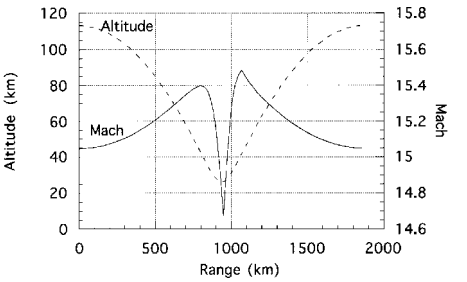

Fig. 4 Altitude and Mach number M, optimal without constraint.

We define a load factor for the vehicle as follows:

$$n = \frac{\sqrt{(T\cos\alpha - D)^2 + (L + T\sin\alpha)^2}}{mg} \tag{27}$$

The load factor defined in Eq. (27) indicates net acceleration/deceleration that the crew experiences in gravitational acceleration; for example, during level flight it becomes 1. High local heating rates and total heating loads are also major concerns in developing a hypersonic transport. Assuming that the optimal trajectory is in the flight regime where boundary-layer theory is valid, the heating rate is estimated at a stagnation point by the following expression,[21] which corresponds to a nose cone with a radius of 10 cm:

$$\dot{Q} = 5.188 \times 10^{-8} \cdot \rho^{0.5} V^3 \tag{28}$$

The maximum calculated load factor and maximum heating rate using Eqs. (27) and (28) are 8.27 g and 1202.4 W/cm^2, respectively. From these estimated results, along the optimal trajectory the heating rate on the nose cone is far beyond the acceptable value unless radiative cooling is available. Thus, a practical optimal solution must include a heating-rate constraint. Before including this constraint, attempt to obtain an optimal solution bounded by a maximum load factor to gain some insights.

Periodic Optimal Control Problem with a Load-Factor Constraint

From Eq. (27) for the load factor, a state-control inequality constraint function $C(\boldsymbol{x}, \boldsymbol{u}, r)$ is defined as

$$C(h, M, s, \alpha) = \frac{\sqrt{(T\cos\alpha - D)^2 + (L + T\sin\alpha)^2}}{mg} - n_{\max} \tag{29}$$

Now the problem is stated as follows.

Find a control and a range period r_f that minimizes the range averaged fuel consumption rate J over the period subject to the vehicle's dynamics, periodicity conditions on the state, and a state-control inequality constraint $C \le 0$. Because convergence is highly sensitive to initial guesses, the exponential atmospheric model is used for this problem:

$$J = \frac{1}{r_f}\int_0^{r_f} \frac{T}{g I_{\rm sp} M a \cos\gamma}\left(1 + \frac{h}{R_0}\right) \mathrm{d}r \tag{30}$$

$$h(0) = h(r_f) \qquad M(0) = M(r_f) \qquad \gamma(0) = \gamma(r_f) \tag{31}$$

$$C(h, M, s, \alpha) \le 0 \tag{32}$$

The augmented Hamiltonian for this system is defined as

$$\bar{H} = \frac{T}{g I_{\rm sp} M a \cos\gamma}\left(1 + \frac{h}{R_0}\right) + \boldsymbol{\lambda}^T \cdot \boldsymbol{f} + \mu^T C \tag{33}$$

where the components of $\boldsymbol{f}$ are Eqs. (1–3). Because C is a scalar function, so is μ. The first-order necessary conditions are obtained simply by replacing H in Eqs. (19–21) and (23) with $\bar{H}$ defined in Eq. (33). On the boundary, α, s, and μ are determined by solving $\bar{H}_\alpha = 0$, $\bar{H}_s = 0$, and $C(h, M, s, \alpha) = 0$ simultaneously. Because there are no analytical solutions for the system of nonlinear equations, a subroutine that uses a modified Powell hybrid algorithm and

a finite difference approximation to the Jacobian is used to solve it numerically. When the standard atmospheric model is used for a problem in which the solution includes a constrained subarc, the sensitivity to initial guesses of the subroutine that solves for α, s, and μ leads to more difficulty than for a problem whose solution is a touch-point type such as the problem in the next section. Because of this, a simple exponential atmospheric model is adopted here. If the calculated s is not in $[0, 1]$, then check $\Delta\bar{H} = \bar{H}(s = 1) - \bar{H}(s = 0)$. If $\Delta\bar{H} \geq 0$, then choose $s = 0$, and if not, choose $s = 1$. For each case, α is determined by solving $C(h, M, s, \alpha) = 0$ and μ is calculated by substituting the values of s and α into $\bar{H}_\alpha = 0$. On the boundary, μ is positive, and when μ becomes zero, exit the boundary. To make use of the optimal periodic solution without constraint that was obtained in the preceding section, we set $n_{\max}$ in C equal to the maximum n for the unconstrained optimal solution. And gradually we decreased the value of $n_{\max}$. After getting several solutions for different values of $n_{\max}$, extrapolation is used to predict a new initial guess of each component of the state and the costate for a new smaller $n_{\max}$. By repeating this procedure we reached an optimal solution with $n_{\max} = 7.0$. Because the change in the maximum load factor from the unconstrained solution was not large, the fuel saving obtained for the solution with $n_{\max} = 7.0$ was almost the same as that for the unconstrained solution. A solution with much smaller $n_{\max}$ than 7.0 has not been obtained due to the difficulty in convergence. Figures 5–8 show the result. Figure 7 is a magnified part of Fig. 6. Figure 8 shows a magnified part of the peak of the profile of the load factor. If the specified maximum load factor is larger than 7.27 g, there appears only one on-boundary arc. But if the maximum load factor is set to smaller than 7.27, another on-boundary arc appears when the engine is turned on. Thus, the solution with $n_{\max} = 7.0$ shows two separate constrained arcs. On the first boundary the throttle stays equal to zero, but on the second boundary the throttle takes middle values between zero and one,

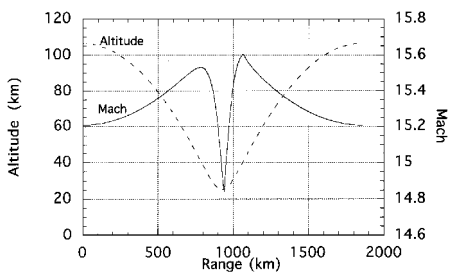

Fig. 5 Altitude and Mach number for $n_{\max} = 7.0$.

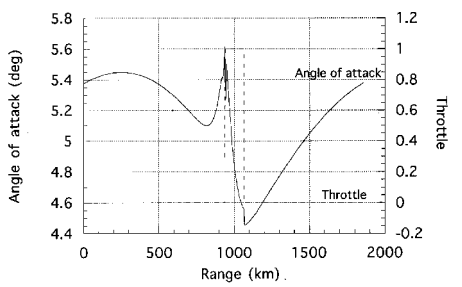

Fig. 6 Angle of attack and throttle for $n_{\max} = 7.0$.

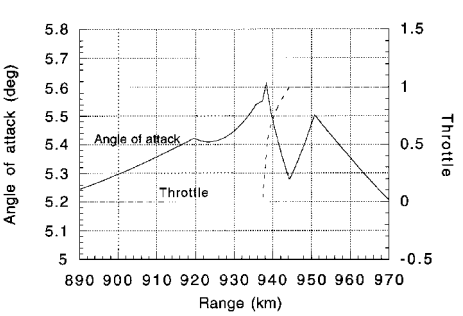

Fig. 7 Angle of attack and throttle for $n_{\max} = 7.0$ (magnified part of Fig. 6).

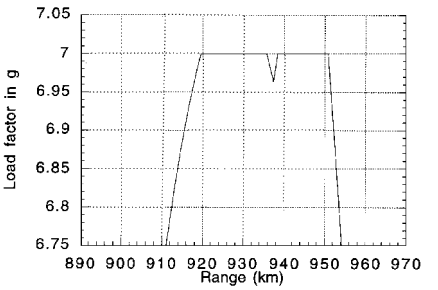

Fig. 8 Load factor for $n_{\max} = 7.0$ (magnified part of the entire profile).

and in the middle point of the boundary the throttle is saturated to one. After that point, the angle of attack α is determined by solving $C(h, M, 1, \alpha) = 0$. Substitution of the calculated $\alpha(s = 1)$ and $s = 1$ into $\bar{H}_\alpha = 0$ determines μ. The boundary conditions of Eq. (22) were solved to seven digits for the solution of this section.

Periodic Optimal Control Problem with a Heating-Rate Constraint

From the expression given by Eq. (28) for the heating rate, a state inequality constraint $S(\boldsymbol{x}, r)$ is explicitly defined as

$$S(h, M) = 5.188 \times 10^{-8} \cdot \rho(h)^{0.5}(Ma)^3 - \dot{Q}_{\max} \tag{34}$$

The fuel-optimal periodic control problem is stated as the following.

Find a control and a range period r_f that minimize the range averaged fuel consumption rate J over the period subject to the vehicle dynamics, periodicity conditions on the state, and a state inequality constraint $S \leq 0$. J and the boundary conditions are the same as Eqs. (30) and (31). Simply exchange inequality (32) with inequality (35):

$$S(h, M) \leq 0 \tag{35}$$

To consider the periodicity conditions Eq. (31) and a state inequality constraint (35) an augmented cost function is defined as

$$\bar{J} = \nu^T[\boldsymbol{x}(0) - \boldsymbol{x}(r_f)] + \pi^T S(x, r)|_{r=r_1} + \frac{1}{r_f}\int_0^{r_f} \frac{T}{gI_{sp}Ma\cos\gamma}\left(1 + \frac{h}{R_0}\right) + \lambda^T\left(\boldsymbol{f} - \frac{\mathrm{d}x}{\mathrm{d}r}\right) + \xi^T\frac{\mathrm{d}S}{\mathrm{d}r}\mathrm{d}r \tag{36}$$

The state inequality constraint here is first order, i.e., a control appears in the equation $\mathrm{d}S/\mathrm{d}r = 0$.

The Hamiltonian for the given augmented cost function $\bar{J}$ is written as

$$\bar{H} = \frac{T}{gI_{sp}Ma\cos\gamma}\left(1 + \frac{h}{R_0}\right) + \lambda^T \cdot \boldsymbol{f} + \xi^T\frac{\mathrm{d}S}{\mathrm{d}r} \tag{37}$$

where the components of $\boldsymbol{f}$ are Eqs. (1–3). The first-order necessary conditions are obtained by substituting $\bar{H}$ for H in Eqs. (19–21) and (23). Other necessary conditions are added for this state inequality problem to ensure that the trajectory meets the specified maximum heating rate at the entry points to the boundary:

$$\lambda\left(r_1^-\right) = \lambda\left(r_1^+\right) + \pi^T\frac{\partial S}{\partial x}\bigg|_{r=r_1} \tag{38}$$

$$H\left(r_1^-\right) = H\left(r_1^+\right) - \pi^T\frac{\partial S}{\partial r}\bigg|_{r=r_1} \tag{39}$$

Because the state constraint S is a scalar, ξ and π are also scalars. From Eq. (38), jumps of costates whose magnitudes are unknown appear at entries to on-boundary sections. On the boundary α, s, and ξ are determined by solving $\bar{H}_\alpha = 0$, $\bar{H}_s = 0$, and $\mathrm{d}S/\mathrm{d}r(h, M, s, \alpha) = 0$ simultaneously. Because there is no analytical solutions for the system of nonlinear equations, the same nonlinear equation solver that was used in the preceding section

is used. As before, if the calculated s is not in [0, 1], then check $\Delta\bar{H} = \bar{H}(s = 1) - \bar{H}(s = 0)$. If $\Delta\bar{H} \geq 0$, then choose $s = 0$, and if not, choose $s = 1$. For each case, α is determined by solving $\mathrm{d}S/\mathrm{d}r(h, M, s, \alpha) = 0$, and ξ is calculated by substituting these s and α into $\bar{H}_\alpha = 0$. On the boundary, ξ is positive and when ξ becomes zero, exit the boundary. If the specified maximum heating rate is larger than approximately 556 W/cm^2, an on-boundary section appears only once before the engine is turned on. But if the maximum heating rate is set smaller than approximately 556 W/cm^2, another on-boundary section appears after the engine is turned on. In this case two different π must be introduced to meet Eq. (38), which makes the problem more difficult to solve. For the problem here the standard atmospheric model is used because the problem turned out to have on-boundary sections whose length is very short. Note that from Eq. (39) the Hamiltonian H is continuous at the entry point r_1 due to the independence of S with respect to r. Thus, the Hamiltonian is constant throughout the period.

As in the preceding section, the optimal periodic solution without constraint is obtained first. The $\dot{Q}_{\max}$ in S is set to the maximum $\dot{Q}$ of the unconstrained optimal solution, which was 1202.4 W/cm^2. Then set a slightly smaller value of $\dot{Q}_{\max}$ to obtain a new optimal solution, which should be close to the original optimal solution without constraint. The obtained solution can be used as a new initial guess for a little smaller $\dot{Q}_{\max}$. By repeating this procedure we can collect several solutions for each distinct $\dot{Q}_{\max}$. Extrapolate these points using the second-, third-, or fourth-order polynomials with respect to values of $\dot{Q}_{\max}$ to predict a new initial guess for a new smaller $\dot{Q}_{\max}$. Finally, an optimal solution for $\dot{Q}_{\max} = 400$ W/cm^2 is obtained. The result is shown in Figs. 9–12. Figure 12 is a magnified part of Fig. 11 by which one can see that the solution appears to be a touch-point solution.

At the beginning of the search for a solution, constrained arcs appear. But as the process converges, the length of the constrained arcs becomes almost a point, which is about 0.015% or less of the length of the period. The first peak of the heating rate is raised by the vehicle's aerobreaking by using its control surface, whereas the second peak is invoked by turning on the engine. The fuel saving for the obtained solution over the steady-state optimal solution is reduced to 2.45%. The boundary conditions of Eq. (22) were solved to eight digits for the solution in this section.

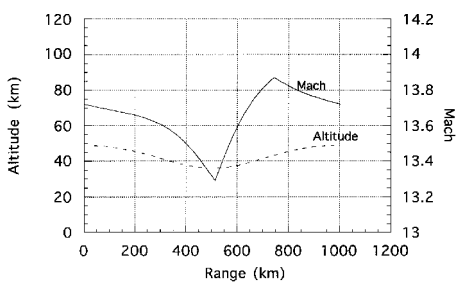

Fig. 9 Altitude and Mach number with $\dot{Q}_{\max}$ = 400 W/cm^2.

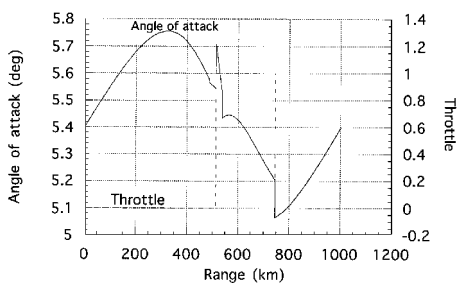

Fig. 10 Angle of attack and throttle with $\dot{Q}_{\max}$ = 400 W/cm^2.

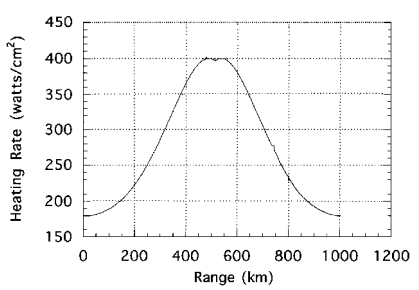

Fig. 11 Heating rate with $\dot{Q}_{\max}$ = 400 W/cm^2.

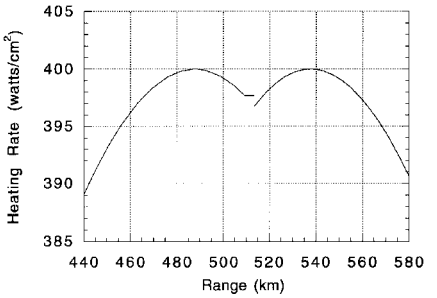

Fig. 12 Heating rate with $\dot{Q}_{\max}$ = 400 W/cm^2 (magnified part of Fig. 11).

Periodic Optimal Control Problem with Both Heating-Rate and Load-Factor Constraints

The fuel-optimal periodic control problem is stated as follows.

Find a control and a range period r_f that minimize the range averaged fuel consumption rate J over the period subject to the vehicle's dynamics, periodicity conditions on the state, a state inequality constraint, and a state-control inequality constraint. J and the boundary conditions on the state are the same as Eqs. (30) and (31). Equations (32) and (35) need to hold along the trajectory. The augmented Hamiltonian is written as

$$\bar{H} = \frac{T}{g I_{\mathrm{sp}} Ma \cos\gamma}\left(1 + \frac{h}{R_0}\right) + \boldsymbol{\lambda}^T \cdot \boldsymbol{f} + \mu^T C + \xi^T \frac{\mathrm{d}S}{\mathrm{d}r} \tag{40}$$

where the components of $\boldsymbol{f}$ are Eqs. (1–3). As before, the first-order necessary conditions are obtained simply by substituting $\bar{H}$ defined in Eq. (40) for H in Eqs. (19–21) and Eq. (23). It is also the same as in the preceding section that other necessary conditions for the state inequality problem are required to ensure that the trajectory meet the specified maximum heating rate at the entry points to the boundary:

$$\boldsymbol{\lambda}\left(r_1^-\right) = \boldsymbol{\lambda}\left(r_1^+\right) + \pi^T \left.\frac{\partial S}{\partial \boldsymbol{x}}\right|_{r=r_1} \tag{38}$$

$$H\left(r_1^-\right) = H\left(r_1^+\right) - \pi^T \left.\frac{\partial S}{\partial r}\right|_{r=r_1} \tag{39}$$

Now there are three types of possible on-boundary sections: 1) boundary subject to a load factor constraint only, 2) boundary subject to a heating rate constraint only, and 3) boundary subject to a load factor and a heating rate constraint. For cases 1 and 2, α, s, μ, and ξ are determined as described in the preceding sections. For case 3 a system of nonlinear equations $\bar{H}_\alpha = 0$, $\bar{H}_s = 0$, $C(h, M, s, \alpha) = 0$, and $\mathrm{d}S/\mathrm{d}r(h, M, s, \alpha) = 0$ must be solved simultaneously.

The only difference from the preceding two sections is that the optimal solution bounded by the maximum heating rate $\dot{Q}_{\max} = 500.0$ W/cm^2 is used as a starting solution. The exponential atmospheric model is used here to decrease the sensitivity. The rest of the procedure is the same. Gradually lower the value of $n_{\max}$ from the original value of $n_{\max}$, which is equal to 2.1693 for the optimal solution bounded by the maximum heating rate $\dot{Q}_{\max} = 500.0$ W/cm^2. By extrapolating the same way as the preceding section, a new initial guess is obtained for a smaller maximum load factor. Finally, the optimal solution subject to $n_{\max} = 2.16$ and $\dot{Q}_{\max} = 500.0$ W/cm^2 was determined. The solution has boundaries of cases 1 and 2. Convergence for a smaller maximum load factor than 2.16 with keeping $\dot{Q}_{\max} = 500.0$ W/cm^2 could not be achieved due to occurrence of a boundary of case 3. The profiles of the altitude and Mach number of the solution look similar to those shown in Fig. 9. The profiles of the angle of attack and throttle are plotted in Fig. 13. Figure 14 is a magnified part of Fig. 13. In Fig. 15 a magnified part of the entire

Table 1 Comparison of each solution

Solution	Fuel improvement over steady-state solution, %	Resulting maximum heating rate, W/cm^2	Resulting maximum load factor
Suboptimal	3.47	513.8	1.58
Optimal without constraint	8.12	1202.4	8.27
Optimal with $n_{max} = 7.0$	8.09	1158.1	7.00
Optimal with $\dot{Q}_{max} = 400$ W/cm^2	2.45	400.0	1.59
Optimal with $n_{max} = 2.16$ and $\dot{Q}_{max} = 500$ W/cm^2	4.03	500.0	2.16

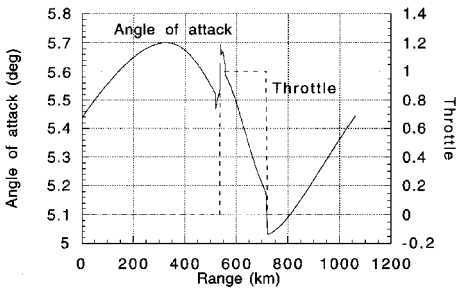

Fig. 13 Angle of attack and throttle with $\dot{Q}_{max} = 500$ W/cm^2 and $n_{max} = 2.16$.

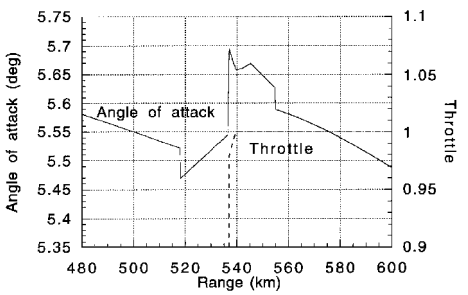

Fig. 14 Angle of attack and throttle with $\dot{Q}_{max} = 500$ W/cm^2 and $n_{max} = 2.16$ (magnified part of Fig. 13).

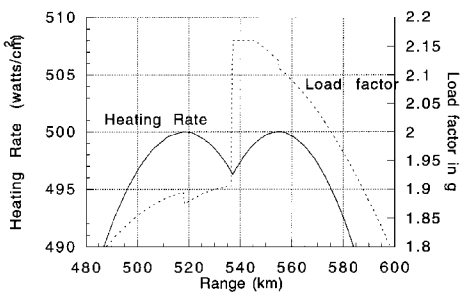

Fig. 15 Heating rate and load factor with $\dot{Q}_{max} = 500$ W/cm^2 and $n_{max} = 2.16$ (magnified part of the entire profiles).

profiles of the heating rate and the load factor, which are not shown here, is plotted. The fuel saving for the obtained solution over the optimal steady-state solution is 4.03%. The boundary conditions (22) were satisfied to seven digits for the solution in this section. The results are summarized in Table 1.

Conclusions

Fuel savings have been shown to be possible for periodic cruise of a hypersonic scramjet vehicle with a reasonable model and practical constraints on the maximum heating rate and the maximum load factor. Numerical solutions are difficult to obtain; however, combinations of the suboptimal approach, the minimizing-boundary-condition method, and a homotopy method have been shown to be effective in reducing the sensitivity to the initial guess for obtaining a solution. Four fuel-optimal periodic solutions have been obtained: one without constraints, one with the load-factor constraint, one with the heating-rate constraint, and one with both the load-factor and the heating-rate constraints. From the solutions obtained here it is observed that the maximum load-factor constraint is coupled with the maximum heating-rate constraint. However, the initial velocities of the solutions with each constraint are quite different. If a load-factor constraint is imposed, the initial velocity of the solution becomes larger than that of the unconstrained solution. When a heating-rate constraint is required to be satisfied, the initial velocity of the solution becomes smaller than that of the unconstrained solution.

Acknowledgment

This study was partially supported by Yokogawa Electric Corporation, Tokyo, Japan.

References

[1]Edelbaum, T., "Maximum Range Flight Paths," United Aircraft Corp., Rept. R-22465-24, East Hartford, CT, 1955.

[2]Bittanti, S., Fronza, G., and Guardabassi, G., "Periodic Control: A Frequency Domain Approach," *IEEE Transactions on Automatic Control*, Vol. AC-18, No. 1, 1973, pp. 33–38.

[3]Speyer, J. L., "Nonoptimality of Steady-State Cruise for Aircraft," *AIAA Journal*, Vol. 14, No. 11, 1976, pp. 1604–1610.

[4]Bernstein, D. S., and Gilbert, E. G., "Optimal Periodic Control: The π Test Revisited," *IEEE Transactions on Automatic Control*, Vol. AC25, No. 4, 1980, pp. 673–684.

[5]Gilbert, E. G., and Lyons, D. T., "Improved Aircraft Cruise by Periodic Control: The Computation of Optimal Specific Range Trajectories," *Proceedings of the Conference on Information Science and Systems*, Princeton Univ. Press, Princeton, NJ, 1980, pp. 602–607.

[6]Colonius, F., "Tests for Properness in Periodic Control of Functional Differential Systems," *Proceedings of the 23rd IEEE Conference on Decision and Control Including the Symposium on Adaptive Processes* (Las Vegas, NV), Inst. of Electrical and Electronics Engineers, New York, 1984, pp. 886, 887.

[7]Speyer, J. L., Dannemiller, D. P., and Walker, D. E., "Periodic Optimal Cruise of an Atmospheric Vehicle," *Journal of Guidance, Control, and Dynamics*, Vol. 8, No. 1, 1985, pp. 31–38.

[8]Grimm, W., Well, K. H., and Oberle, H. J., "Periodic Control for Minimum-Fuel Aircraft Trajectories," *Journal of Guidance, Control, and Dynamics*, Vol. 9, No. 2, 1986, pp. 169–174.

[9]Breakwell, J. V., "Oscillatory Cruise—A Perspective," *Optimal Control*, Vol. 95, Lecture Notes in Control and Information Sciences, Springer–Verlag, Berlin, 1987, pp. 157–168.

[10]Chuang, C.-H., and Speyer, J. L., "Periodic Optimal Hypersonic Scramjet Cruise," *Optimal Control Applications and Methods*, Vol. 8, July–Sept. 1987, pp. 231–242.

[11]Menon, P. K. A., "Study of Aircraft Cruise," *Journal of Guidance, Control, and Dynamics*, Vol. 12, No. 5, 1989, pp. 631–639.

[12]Sachs, G., and Lesch, K., "Periodic Maximum Range Cruise with Singular Control," *Journal of Guidance, Control, and Dynamics*, Vol. 16, No. 4, 1993, pp. 790–793.

[13]Dewell, L. D., and Speyer, J. L., "An Investigation of the Fuel-Optimal Periodic Trajectories of a Hypersonic Vehicle," *Proceedings of the AIAA Guidance, Navigation, and Control Conference* (Monterey, CA), AIAA, Washington, DC, 1993, pp. 466–473 (AIAA Paper 93-3753).

[14]Anderson, J. D., *Introduction to Flight*, 3rd ed., McGraw–Hill, New York, 1989, p. 74.

[15]Ware, G. M., and Cruz, C. I., "Aerodynamic Characteristics of the HL-20," *Journal of Spacecraft and Rockets*, Vol. 30, No. 5, 1993, pp. 529–536.

[16]Shaughnessy, J. D., Pinckney, S. Z., McMinn, J. D., Cruz, C. I., and Kelley, M.-L., "Hypersonic Vehicle Simulation Model: Winged-Cone Configuration," NASA TM 102610, Nov. 1990.

[17]Penland, J. A., Marcum, D. C., Jr., and Stack, S. H., "Wall-Temperature Effects on the Aerodynamics of a Hydrogen-Fueled Transport Concept in Mach 8 Blowdown and Shock Tunnels," NASA TP 2159, July 1983.

[18]Eguchi, K., Fujiwara, T., Yamanaka, T., Miki, Y., Tokunaga, T., and Togawa, M., "An Advanced SCRAMjet Propulsion Concept for a 350 Mg SSTO Space Plane External Nozzle Performance," AIAA Paper 92-3719, July 1992.

[19]Tsujikawa, Y., and Nagaoka, M., "Determination of Cycle Configuration of Gas Turbines and Aircraft Engines by an Optimization Procedure," *Journal of Engineering for Gas Turbines and Power*, Vol. 113, No. 1, 1991, pp. 100–105.

[20]Kato, K., *Space Plane*, Tokyo Univ. Press, Tokyo, Japan, 1989, pp. 144–148 (in Japanese).

[21]Tauber, M. E., and Menees, G. P., "Aerothermodynamics of Transatmospheric Vehicles," *Journal of Aircraft*, Vol. 24, No. 9, 1987, pp. 594–602.

F. H. Lutze Jr.
Associate Editor